Thermal Fractionation and Isothermal Crystallization of Polyethylene Nanocomposites Prepared by in Situ Polymerization

M. Trujillo, M. L. Arnal, and A. J. Müller*

Grupo de Polímeros USB, Departamento de Ciencia de los Materiales, Universidad Simón Bolívar, Apartado 89000, Caracas 1080-A, Venezuela

St. Bredeau, D. Bonduel, and Ph. Dubois

Service des Matériaux Polymerès et Composites SMPC, Center of Research and Innovation in Materials & Polymers CIRMAP, Université de Mons-Hainaut, Place du Parc 20, B-7000 Mons, Belgium

I. W. Hamley and V. Castelletto

School of Chemistry, University of Reading, Whiteknights, Reading RG6 6AD, U.K.

Received October 11, 2007; Revised Manuscript Received January 7, 2008

ABSTRACT: Nanocomposites of high-density polyethylene (HDPE) and carbon nanotubes (CNT) of different geometries (single wall, double wall, and multiwall; SWNT, DWNT, and MWNT) were prepared by in situ polymerization of ethylene on CNT whose surface had been previously treated with a metallocene catalytic system. In this work, we have studied the effects of applying the successive self-nucleation and annealing thermal fractionation technique (SSA) to the nanocomposites and have also determined the influence of composition and type of CNT on the isothermal crystallization behavior of the HDPE. SSA results indicate that all types of CNT induce the formation of a population of thicker lamellar crystals that melt at higher temperatures as compared to the crystals formed in neat HDPE prepared under the same catalytic and polymerization conditions and subjected to the same SSA treatment. Furthermore, the peculiar morphology induced by the CNT on the HDPE matrix allows the resolution of thermal fractionation to be much better. The isothermal crystallization results indicated that the strong nucleation effect caused by CNT reduced the supercooling needed for crystallization. The interaction between the HDPE chains and the surface of the CNT is probably very strong as judged by the results obtained, even though it is only physical in nature. When the total crystallinity achieved during isothermal crystallization is considered as a function of CNT content, it was found that a competition between nucleation and topological confinement could account for the results. At low CNT content the crystallinity increases (because of the nucleating effect of CNT on HDPE), however, at higher CNT content there is a dramatic reduction in crystallinity reflecting the increased confinement experienced by the HDPE chains at the interfaces which are extremely large in these nanocomposites. Another consequence of these strong interactions is the remarkable decrease in Avrami index as CNT content increases. When the Avrami index reduces to 1 or lower, nucleation dominates the overall kinetics as a consequence of confinement effects. Wide-angle X-ray experiments were performed at a high-energy synchrotron source and demonstrated that no change in the orthorhombic unit cell of HDPE occurred during crystallization with or without CNT.

1. Introduction

Carbon nanotubes (CNT) are considered excellent reinforcing fillers because of the outstanding properties that they can induce when adequately dispersed in polymeric matrices, such as rigidity increases without important losses in ductility and enhancement in electrical conductivity. These properties are intimately connected with the extremely high aspect ratio of CNT which facilitate the establishment of percolation paths in the case of good dispersions.[1−4]

However, the achievement of good dispersions is not an easy task. Several CNT dispersion routes into polymeric matrices have been described in the literature such as solution blending, melt mixing and in situ polymerization.[4] Recently, Dubois et al.[5] developed a method derived from the polymerization-filling technique (PFT) initially employed in Ziegler−Natta polymerization processes[6,7] and more recently adapted for the application of metallocenic catalysts to a wide range of microfillers, such as kaolin, silica, wollastonite, graphite, and glass microspheres[8−11]. A highly active metallocenic complex is physico-chemically grafted to the CNT surfaces before the in situ polymerization of ethylene takes place. Since the polyethylene (PE) chains grow on the surface of CNT, a good dispersion is easily achieved by disaggregation. The in situ nanocomposite obtained can be used as polymerized or as a masterbatch that could be blended with PE-based resins to form nanocomposites of varying compositions.

The excellent properties of the nanocomposites are a function of the interface characteristics which in turn are determined by the superficial energy of the fillers. A good interface adhesion is achieved when the superficial energy of the filler is larger than the cohesive energy of the matrix. In the case of nanofillers, because of their small size and high aspect ratio, the percentage of atoms that are exposed on the interface can be as high as 50% of the total atoms in the nanofiller. This peculiar characteristic increases the superficial energy of the nanofillers and favors a higher interaction between the filler and the matrix.[12] In the preparation of CNT/polymer nanocomposites the establishment of interactions between the components can be favored by physisorption phenomena (i.e., multiple contacts

* Corresponding author.

10.1021/ma702272e CCC: $40.75
Published on Web 02/19/2008

between the polymer chains and the CNT surface that may even provoke entanglement formation of the polymer chains around the nanotubes) or chemisorption if specific interactions can be developed.[13]

The presence of interactions between CNT and the polymeric matrix can cause alterations in the crystallization and melting process of the polymer in question. In particular for polyolefins several effects have been reported in the literature. Haggenmüller at al.[14] have performed a detailed study of PE/SWNT (single wall nanotubes) nanocomposites prepared by a hot coagulation method. They have found that SWNT bundles can act as nucleation agents for PE and they also affect the superstructural morphology inducing a change from three-dimensional spherulites to two-dimensional disks. The chains crystallize in lamellae that are perpendicular to the SWNT bundles; therefore, the PE chains are oriented parallel to the SWNT.

Bhattachary et al.[15] have shown that only 0.8% by weight of SWNT is capable of nucleating isotactic polypropylene (PP) with the consequent reduction in spherulitic size and in the times needed to achieve 50% of its crystallization. Grady et al.[16] also reported a nucleating effect of CNT on PP during isothermal crystallization studies and a preferential formation of the β crystalline phase over the more common α phase. On the other hand, Assouline and co-workers[17] reported a nucleating effect of CNT on the PP α phase. Nanocomposites incorporating SWNT in a poly(vinyl alcohol), PVA, matrix have also been prepared and a nucleating effect was also detected under nonisothermal conditions.[18] Minus et al.[19] corroborated this nucleation phenomena and also claimed that the polymer chains oriented parallel to the CNT surfaces.

Michell and Krishnamoorti[20] prepared polycaprolactone and functionalized SWNT nanocomposites and found that the SWNT act as strong nucleating agents that can accelerate the overall crystallization rate under nonisothermal conditions. However, the crystal unit cell of PCL, its melting point and crystallinity were not affected by the SWNT inclusion. On the other hand, Ryan et al.[21] prepared a conjugated polymer-based composite combining poly(*m*-phenylenevinylene-*co*-2,5-dioctyloxy-*p*-phenylenevinylene (PmPV) with multiwall nanotubes (MWNT). They also report the nucleating action of MWNT but observed increases in crystallinity and melting point with MWNT content. In fact, their composite material melts with a double peak and they attribute the highest temperature melting peak to the fusion of the crystals nucleated by the MWNT.

Contrary to the previous works cited above, other researchers have reported reductions on the crystallization and melting points of polymeric matrices loaded with CNT.[13,22] In the case of poly(ethylene oxide)/functionalized CNT nanocomposites, it has been reported that the thermal properties do not experience any significant variation with respect to the homopolymer for SWNT concentrations up to 7%,[23] while more recently, Chatterjee et al.[24] reported for a similar system reductions in the melting point and crystallinity of PEO with the addition of 0.1 to 2% SWNT.

In a previous work,[25] we have examined the thermal behavior and the morphology of PE/CNT nanocomposites prepared by the in situ polymerization method of Dubois et al. The effects of composition (5−22% CNT by weight) and structure of the nanotube (single wall, double wall, or multiwall; i.e., SWNT, DWNT, or MWNT) were evaluated and an excellent nucleating effect (both during dynamic and isothermal crystallization conditions) on polyethylene matrix was found regardless of the CNT type in comparison to neat high-density polyethylene (HDPE) polymerized under identical conditions. Self-nucleation studies demonstrated that CNT were more efficient in nucleating the HDPE than its own crystal fragments. According to differential scanning calorimetry (DSC) and transmission electron microscopy (TEM) results, the crystals produced within the nanocomposite HDPE matrix were more stable than those produced in neat HDPE or in physical blends prepared by melt mixing of HDPE and untreated CNT. Melting points up to 5 °C higher than neat HDPE were encountered in the nanocomposites as well as consequently thicker lamellae. Furthermore, a bottle-brush morphology was revealed by TEM indicating that the chains near the CNT surfaces were oriented parallel to the CNT axis.

We can summarize the above by stating that the effects of CNT on the nucleation of several polymers have been studied and in general four different trends have been reported:

(1) A classical nucleation agent effect of CNT on the polymer matrix has been found for isotactic polypropylene,[15−17,26] poly(ethylene tereftalate),[27−28] polycaprolactone,[20,29] poly(vinyl alcohol),[18−19] poly(*m*-phenylenevinylene-*co*-2,5-dioctyloxy-*p*-phenylenevinylene)[21] and polyethylene.[14] The quoted works reported increases in crystallization temperature, enhances in nucleation density and in some cases reduction of crystallization times.

(2) No effect of CNT on the nucleation of polymer crystals has been reported.[23] Goh et al. employed a double-C60-end-capped poly(ethylene oxide) reinforced with acid treated MWNT's and found that the crystallization behavior was not significantly affected by the MWNT's.

(3) Results that could be classified as anti-nucleation effects of CNT have also been reported in the literature. Chatterjee et al.[24] have prepared surfactant assisted dispersions of SWNT's in poly(ethylene oxide), PEO, and found reductions in both melting temperature and crystallinity with increases in SWNT contents. Jin et al.[30] have found a reduction in nucleation density in PEO/chemically modified MWNT's nanocomposites as well as reductions in PEO crystallinity. In the references quoted above for the three cases reported so far, the loading of CNT was usually restricted to values of 1% or lower (except in a few cases were contents in the range 1−4.6% were employed, e.g., 1.6%,[16] 1.4% and 3%,[21] 1.8 and 4.6%,[20] 2%[28]).

(4) An exceptionally high nucleation effect induced by the CNT−polymer interface morphology observed for in situ polymerized polyethylene on treated CNT, where PE chains grow with a bottle brush lamellar morphology on the surface of CNT that contain physicochemically attached metallocene catalysts.[25] In this previous work where we employed the same materials studied in this paper, the nucleation effect induced by CNT (in a proportion of 6−10% by weight) was even higher than that induced by polyethylene self-nuclei. The remarkable nucleating effect decreased as the CNT content was increased to very high levels (from 6% to 30%).

In this work, we further explore the nucleation ability of CNT on PE/CNT nanocomposites that have been well characterized from a morphological point of view in a preceding paper[25] by examining their ability to modify the crystallization kinetics of the PE matrix. Samples including large quantities of CNT are also examined and large changes in their crystallization ability and nucleation mechanisms could be envisaged. Furthermore, we investigate the thermal fractionation behavior of the PE with and without treated CNT since the fractionation behavior relates to the ability of the chains to molecularly segregate depending on their crystallization temperature. Since the interactions between chains and CNT may affect molecular mobility and alignment near the PE/CNT extremely large interface, then a substantial effect on the fractionation ability may be expected.

Table 1. HDPE/CNT Nanocomposites Evaluated: HDPE/SWNT ($PE_xS_yA_z$), HDPE/DWNT ($PE_xD_yA_z$), and HDPEE/MWNT ($PE_xM_yA_z$)

composition	type	CNT content (%)	HDPE content (%)	Al_2O_3 content (%)
HDPE			92.4	7.60
$PE_{87}S_8A_5$	SWNT	7.57	87.07	5.36
$PE_{56}S_{20}A_{24}$	SWNT	20.05	56.08	23.87
$PE_{33}S_{36}A_{31}$	SWNT	33.21	36.21	30.58
$PE_{82}D_8A_{10}$	DWNT	7.6	82.20	10.17
$PE_{60}D_{17}A_{23}$	DWNT	17.35	60.16	22.49
$PE_{44}D_{26}A_{30}$	DWNT	26.19	43.45	30.36
$PE_{83}M_6A_{11}$	MWNT	5.91	82.55	11.53
$PE_{68}M_{11}A_{21}$	MWNT	11.15	68.21	20.64
$PE_{41}M_{26}A_{33}$	MWNT	26.41	41.06	32.53

2. Experimental Section

2.1. Sample Preparation. The HDPE/CNT nanocomposites were prepared by a soft method derived from the polymerization-filling technique (PFT) using metallocene catalysis. Methylaluminoxane (MAO), a well-known cocatalyst used in metallocene-based olefin polymerization process, was anchored onto the surface of CNT in suspension in dried heptane. The metallocene catalyst employed here was bis(pentamethyl-η^5-cyclopentadienyl)zirconium(IV) dichloride ($Cp^*_2ZrCl_2$, where Cp* where Cp stands for cyclopentadienyl), which was then reacted with the surface-activated carbon nanotubes. The addition of ethylene yields the synthesis of polyethylene (HDPE) exclusively at the surface of the CNT. The PE coating limits the formation of airborne carbon nanotubes aggregates, making handling much safer. Detailed description of the polymerization process is presented in ref 5 and 31.

Table 1 show the composition and identification of all the samples employed. For comparison purposes a neat HDPE homopolymer was synthesized using similar conditions to those employed for the nanocomposites. Three types of CNT were used: single wall (SWNT), double wall (DWNT), and multiwall (MWNT). The following nomenclature is used to indicate the composition of the samples: $PE_xS_yAl_z$ where the subscripts indicate the percent by weight contents of each component present in the formulation (HDPE, CNT, and Al_2O_3 respectively), the letter S is used to denote SWNT, other samples with letters D or M indicate DWNT or MWNT. The compositions were determined by Thermogravimetry analysis (TGA). Table 1 show that the CNT are present in the samples in three different contents: low (5−8%), medium (11−20%) and high (26−33%). The highest contents of CNT are present in SWNT systems. The diameters of the CNT employed were determined by TEM and the results yield: 2, 4, and 5−27 nm for SWNT, DWNT, and MWNT, respectively.

2.2. Thermal Characterization. Differential scanning calorimetry (DSC) was performed with a Perkin-Elmer Pyris 1 instrument calibrated with indium and tin under an ultrahigh purity nitrogen atmosphere. Sample weights of approximately 5 mg were employed and the samples were encapsulated in aluminum pans and sealed. The crystalline thermal history was erased by heating the samples at 170 °C for 3 min.[32] Cooling and subsequent heating scans were registered at 10 °C/min.

Successive Self-Nucleation and Annealing Experiments (SSA). In order to evaluate the nucleation capacity of CNT on HDPE, self-nucleation tests (SN) were performed in a preceding work[25] according to procedures devised originally by Fillon et al.[32−34] The SSA technique was developed by Müller et al. and has been recently reviewed.[34−39] It is basically a thermal fractionation technique that promotes the potential molecular fractionation that occurs during crystallization, while encouraging annealing of the unmolten crystals at each stage of the process, so that small effects can be magnified. The complete thermal treatment comprises the following:

(a) Erasure of crystalline thermal history by heating the sample to 170 °C for 3 min;

(b) Creation of a "standard" thermal history by cooling at 10 °C/min to 25 °C;

(c) DSC heating scan from room temperature to a partial melting temperature denoted T_s;

(d) Isothermal step for 5 min at T_s;

(e) DSC cooling scan from T_s, where the effects of the thermal treatment will be reflected on the crystallization of the HDPE;

(f) Final melting, where the sample was heated at 10 °C/min from 0 to 140 °C and a multiple melting endotherm was obtained.

The first T_s temperature to be used in step "d" should be carefully chosen. It is generally advisable to employ the lowest T_s temperature within Domain II (or self-nucleation Domain[32−39]) of the polymer taken as a standard for comparisons to be made. This means that the first T_s will only cause self-nucleation but not annealing. In our case, HDPE was our internal standard for later comparisons. HDPE is characterized by an extremely high heterogeneous nuclei density. This makes difficult the appreciation of domain II, and in the present case, it was not detected. Therefore, for the HDPE employed in this work, a transition from domain I to domain III (from complete melting domain to self-nucleation and annealing domain[32−39]) was directly observed at 131 °C. Therefore, a T_s temperature of 133 °C was chosen, which was located just below domain I, already at the beginning of domain III.

Steps "c" to "e" of the SSA method described above were repeated at increasingly lower T_s. The differences in T_s were always kept constant at 5 °C. The number of repetitions can be chosen to cover the entire melting range of the sample with a "standard" thermal history or a shorter range. In order to maintain a standard thermal treatment based on the homopolymer, the SSA procedure was performed for all the samples, choosing a T_s of 133 °C, for the first thermal treatment, and the T_s temperatures were varied from 133 to 98 °C at 5 °C intervals for a total of eight self-nucleation/annealing steps. We have previously studied in an earlier publication the self-nucleation behavior of the samples employed here[25] and in that reference the temperatures at which the transition between regimes I and III occur are also reported.

Isothermal Crystallization Kinetics. The samples were first heated to 170 °C and kept in the melt for 3 min, in order to erase all crystalline thermal history, before they were quenched (at 60 °C/min) to the chosen isothermal crystallization temperature, T_c. In order to choose the T_c range, tests were run by quenching the sample to a specific T_c and then immediately heating it while recording its heating scan at 10 °C/min. If any melting was observed, it indicated that the sample was able to crystallize during the previous quenching at 60 °C/min. Therefore, this T_c was not employed and the test was repeated at higher temperatures until no crystallization during the quenching was obtained. This procedure was used to find the lowest T_c, then isothermal crystallization experiments were run every half a degree from that T_c upward in temperature until the crystallization exotherm was too small to be detected by the DSC. This procedure is the usual to obtain continuous isothermal crystallization (CIC) data with the DSC.

In some cases, the latent heat of isothermal crystallization was so small that it was impossible to detect during a CIC experiment. In those cases, we employed the isothermal step crystallization experiments (ISC); see ref 40. The samples were quenched to T_c at 60 °C/min and then a specific crystallization time was observed; after this time had elapsed, a DSC scan was registered from T_c until full melting was achieved. The melting enthalpy was then taken as equivalent to the crystallization enthalpy for that specific time. The procedure was repeated for as many crystallization times were needed in order to describe a full enthalpy of melting vs time curve which would allow for crystallization kinetic calculations with the Avrami equation.[41]

2.3. X-ray Evaluation. Simultaneous small-angle and wide-angle X-ray scattering experiments were performed on station 6.2 at the Synchrotron Radiation Source, Daresbury Lab., U.K. Samples contained in DSC pans modified to incorporate mica windows to allow transmission of the X-ray beam were mounted in a Linkam DSC cell of single pan design for thermal treatment. The X-ray wavelength was $\lambda = 1.40$ Å. SAXS data were collected with a RAPID multiwire quadrant detector and the WAXS detector had a curved multiwire design. The wavenumber $q = 4\pi(\sin\theta)/\lambda$ for SAXS was calibrated using rat-tail collagen, and the WAXS angular scale was calibrated using high-density polyethylene (HDPE).

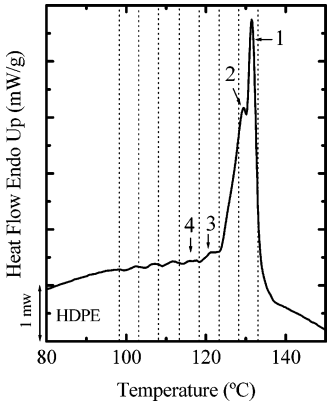

Figure 1. DSC heating scan at 10 °C/min for HDPE after SSA thermal fractionation.

SAXS data were registered with a RAPID multiwire quadrant detector and the WAXS detector had a curved multiwire design. WAXS patterns were taken isothermally as the sample crystallized trying to match the same procedure employed for CIC in the DSC.

3. Results and Discussion

A detailed analysis of the thermal behavior of the samples described in Table 1 was presented previously (see ref 25). The results clearly indicated the strong nucleating effect that CNT induce on the HDPE matrix. Also, the more stable nature of the HDPE crystals produced when the nanocomposites are prepared by in situ polymerization was indicated by the higher melting points exhibited in comparison with neat HDPE or with the $PE_{93}M_6A_1$* system, which was prepared by melt mixing HDPE and MWNT without any treatment.

Because of the synthesis procedure employed, residual alumina is always present in the nanocomposites (see ref 5 and 31) and its content increases with CNT, as can be seen in Table 1. It was found in ref 25 that the degree of crystallinity decreases monotonically as the amount of CNT increases. This is unexpected since nucleating agents normally do not affect crystallinity or tend to increase it; however, the amounts of nucleating agents usually employed rarely exceed 3%. In this case, the decrease in crystallinity is certainly more pronounced at higher CNT concentrations. CNT possess a remarkably high superficial area, therefore, at high contents they are probably interfering with crystal growth, especially when the extremely high number of nucleating sites they provide are taken into account. When CNT content increases, the amount of Al_2O_3 residues also increases. Therefore, the PE phase can amount to just 30−50% of the material. At such high loads of fillers (both CNT and alumina), the interference with the crystal growth process is very important.

3.1. Successive Self-Nucleation and Annealing Behavior. As explained in the experimental part, the first T_s temperature chosen corresponded to 133 °C, this is 2 °C above the frontier between domains I and III for HDPE.[25] The total number of fractionation steps applied was 8, employing a fractionation window of 5 °C in regular intervals from 133 °C until 98 °C.

The final heating scan after SSA fractionation for neat HDPE is shown in Figure 1. It exhibits two dominating endotherms (labeled 1 and 2 in Figure 1) whose melting peaks are very close to each other (131.6 and 129.6 °C) and are the product of the thermal fractionation achieved during the first three fractionations steps applied (i.e., 133, 128 and 123 °C were the first three T_s temperatures applied, the first fractionation step only causes self-nucleation in HDPE, while the other two produce self-nucleation plus annealing and therefore generate

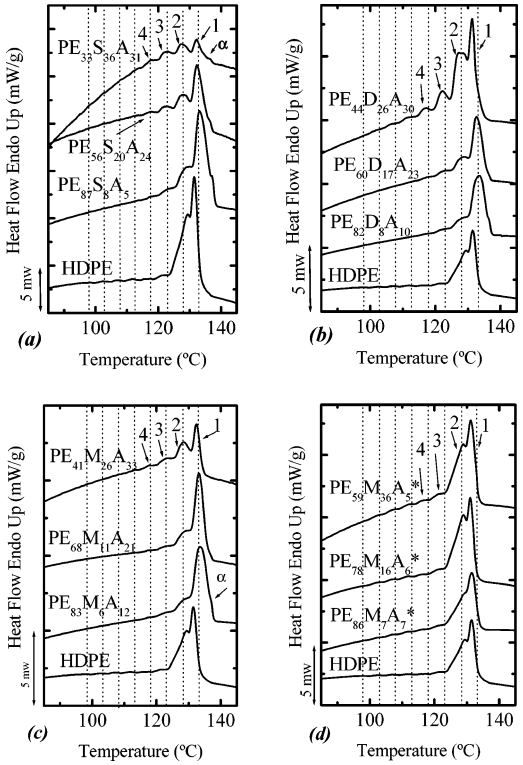

Figure 2. DSC heating scans at 10 °C/min after SSA thermal treatment fractionation: (a) $PE_xS_yA_z$, (b) $PE_xD_yA_z$, (c) $PE_xM_yA_z$, (d) $PE_xM_yA_z$*.

the fractions 1 and 2). These two thermal fractions represent 80% of the total melting endotherm of the material. The rest of the thermal fractions produced are five small endotherms clearly defined by the other five T_s temperatures applied, but they are less important in magnitude (only the first four thermal fractions produced are labeled with 1, 2, 3, and 4 in Figure 1). The final shape of the heating scan after SSA can be regarded as consistent with a highly regular linear HDPE where 80% of the crystallizable methylene linear portions of the chain fall into two fractions (fractions 1 and 2, where the thicker crystals containing the longest methylene sequences melt) and the rest corresponds to increasingly shorter methylene sequences. The thermal fractionation in the absence of branches in polyethylene chains proceeds by differences in molecular weights between the constituent chains and is not as efficient as when the polymer contains short chain branches, like in ethylene/α-olefin copolymers. The thermal fractionation of analogous HDPE materials has already been reported in the literature with similar results.[34,38,39]

The results of applying the same SSA treatment to the in situ nanocomposites containing different amounts of CNT are shown in Figure 2 and marked differences can be observed when a comparison is made with thermally fractionated HDPE. One of the most important differences is the appearance of a new high-temperature fraction which is not present in the HDPE (this has been labeled α in the top DSC scan shown in Figure 2a for $PE_{33}S_{36}A_{31}$). This new fraction is consistent with the results of reference 25 that report higher melting points for the nanocomposites (especially at low CNT contents) as compared to HDPE as well as higher domain I to domain III transition temperatures.[25] Since the SSA protocol was the same for HDPE and the nanocomposites, the logical outcome is the production of a higher melting fraction in the PE/CNT in situ nanocomposites. The first T_s treatment at 133 °C produces the annealed fraction α (absent in HDPE), which can be observed in Figure 2 for the following nanocomposites: $PE_{87}S_8A_5$, $PE_{56}S_{20}A_{24}$, $PE_{33}S_{36}A_{31}$,

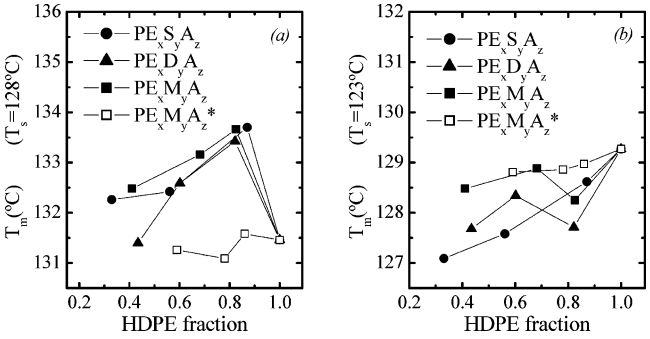

Figure 3. (a) Melting points of thermal fractions number 1 as a function of HDPE content for the nanocomposite systems. (b) Melting points of thermal fractions number 2 as a function of HDPE content for the nanocomposite systems.

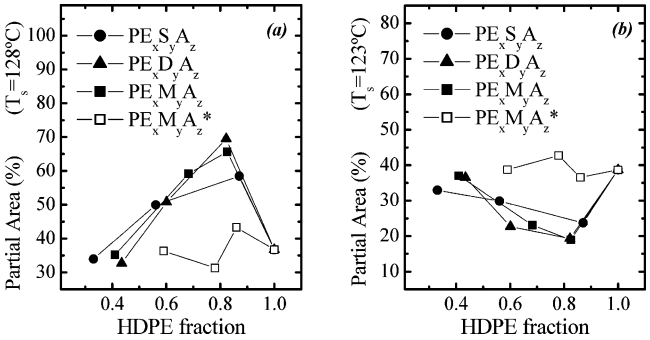

Figure 4. (a) Partial melting areas of thermal fractions number 1 as a function of HDPE content for the nanocomposite systems. (b) Partial melting areas of thermal fractions number 2 as a function of HDPE content for the nanocomposite systems.

$PE_{82}D_8A_{10}$, $PE_{60}D_{17}A_{23}$, $PE_{83}M_6A_{12}$, $PE_{68}M_{11}A_{21}$ (see Figure 2, parts a, b, and c). Figure 2d shows that if a HDPE/MWNT blend is prepared by melt blending (without any treatment on the CNT surface) the special morphology produced during the in situ polymerization method is not formed and basically the matrix remains identical to neat HDPE and therefore the SSA thermal fractionation does not produce fraction α and all DSC scans in Figure 2d are very similar to that of neat HDPE after SSA (compare with Figure 1).

Figure 3a plots the variation of peak melting points of thermal fraction 1 with HDPE content in the nanocomposites, while Figure 3b does the same with thermal fraction 2. It can be clearly observed how the melting point of thermal fraction 1 is substantially increased in the in situ prepared nanocomposites as compared to its value in neat HDPE, especially when the content of CNT is low. At the same time the melting point of fraction number 2 correspondingly decreases. For comparison purposes, the values obtained with the physical blend of MWNT and HDPE are presented and they do not show any significant variation with CNT content within the experimental error of the measurements.

In Figure 2, it can also be appreciated that the area under the endotherm corresponding to fraction 1 increases in the in situ prepared nanocomposites as compared to the area under fraction number 1 in neat HDPE (compare with Figure 1). The effect is more noticeable in the compositions with lower amounts of CNT, a fact that is also consistent with the results obtained in the standard DSC scans, where always the samples with lower amounts of CNT exhibited higher melting points (see Table 1). The results of the partial areas measurements (i.e., the approximate area under each melting peak) are shown in Figure 4. Figure 4a shows a plot of the variation of the area under peak 1 or thermal fraction 1 with the HDPE content, while Figure 4b shows an equivalent plot for thermal fraction 2. It can be observed that as the area or amount of fraction 1 increases a corresponding decrease in the amount of fraction 2 occurs. Also, the effect is more pronounced when the content of CNT is low and tends to disappear at very high CNT contents. These SSA results are consistent with the thermal behavior previously reported in ref 25, where the effects of melting point enhancement by the CNT also tend to disappear at high CNT content when the quantity of HDPE decreases, also the crystallinity of the HDPE matrix decreases as the CNT content increases.

A novel result obtained by SSA and reported in Figure 2 is that a change in the distribution of melting points in the in situ nanocomposites has occurred as compared to neat HDPE and the change is much more noticeable as the content of CNT increases. The results indicate that in those in situ nanocomposites with 20% nanotubes or more (this means also that they contain a high content of alumina, typically more than 24%, a byproduct of the synthesis, see ref 25), where the PE phase amounts to only 56% or lower a change in the fractionation resolution has been achieved. The melting peaks corresponding to fractions 1 and 2 are more spaced in temperature in the systems containing CNT than in HDPE, probably because the melting point of fraction 1 has been increased while the melting temperature of fraction 2 does not increase (or even slightly decrease), as can be seen in Figure 3, parts a and b.

It is not clear why the fractionation becomes so much better in those samples containing large amounts of CNT and alumina. We assume that the molecular weight as well as the molecular structure (absence of branches) remain unaltered in all the samples since the polymerization conditions are the same. If this is true, then the changes in fractionation can only be attributed to the peculiar morphologies (and chain conformations) induced by a high amount of CNT. These variations in the shape of the multiple endotherm and partial areas distribution must then be a consequence of the nanotubes presence. Since they possess a small diameter and high aspect ratio, CNTs create a network within the polymer at high contents that interfere with crystal growth (in fact the total crystallinity of the samples decreases with CNT content). Apparently such growth restrictions affect more the thickest crystals formed in fraction 1 and therefore, fraction 2, which melts at lower temperatures gains importance as the CNT content increases. Unfortunately, it is very difficult (if not impossible) to separate the HDPE from the CNT (and alumina), a fact that accounts why we were unable to run size exclusion chromtaography (SEC) experiments with the nanocomposite samples.

As mentioned previously, the SSA treatment was also applied to a physical blend of HDPE and MWNT of analogous compositions to the in situ prepared nanocomposites. The results are also shown in Figures 2, 3, and 4. The behavior is totally different to that exhibited by the in situ nanocomposites. In this case, the shape of the multimodal endotherm is comparable within the experimental error to that observed for HDPE. In this case, the MWNT mechanically incorporated in HDPE in the melt do not promote the formation of more stable thicker lamellae that melt at higher temperatures. In this blend the dispersion obtained is not very good since the disaggregation characteristic of the in situ polymerization is not present.

The results of applying the SSA thermal fractionation to the nanocomposites prepared by in situ polymerization corroborate the findings reported in ref 25 with TEM and standard DSC experiments since the fractions that melt at the highest temperatures (i.e., fraction labeled number 1 in Figure 2) in all systems with CNT have a higher melting point than in neat HDPE. SSA

applies successive self-nucleation and annealing steps that are designed to produce the thickest possible lamellar thicknesses since the crystals are stabilized by the successive annealing steps, and in the end, these crystals are much closer to equilibrium than those formed in the untreated material. It is therefore interesting that once more we have evidence indicating that lamellar crystals formed during the SSA treatment (corresponding to the highest melting thermal fraction) in samples with CNT formed thicker and more stable crystals than those produced under equivalent conditions in neat HDPE.

3.2. Isothermal Crystallization. The isothermal crystallization of all samples was determined by DSC and the results were fitted with the Avrami equation,[41] a common tool to describe overall isothermal crystallization (including nucleation and growth). According to Avrami:[41]

$$1 - V_c(t) = \exp(-K t^n) \quad (1)$$

where V_c is the relative transformed volume fraction at the crystallization time t; K is the overall crystallization rate constant which is a function of nucleation and growth and n is the Avrami index. The Avrami index is a complex exponent whose value is related to the dimensionality of the growing crystals and to the time dependence of nucleation.[41] The fittings of the data to the Avrami equation were performed following closely the procedure established in ref 42.

Figure 5a shows the evolution of the Avrami index (n) with isothermal crystallization temperature for several *in situ* nanocomposites. In the case of nanocomposites with low amounts of CNT, the Avrami index fluctuates in between 1.9 and 2.4. This corresponds approximately to an Avrami index of 2 which can be interpreted as arising from the instantaneous nucleation of bidimensional structures (e.g., axialites). This result is consistent with the high density of nuclei that this HDPE possesses. In fact self-nucleation experiments demonstrated[25] that domain II does not exist in this polymer because of the high intrinsic nucleation density. The slight increase in the Avrami index with temperature observed for several systems may be due to either a change in nucleation from instantaneous to sporadic or to a dimensionality change (from 2D to 3D structures). The nanocomposites were able to crystallize at lower supercoolings than neat HDPE as a consequence of the important nucleating action of CNT on HDPE (see also Figure 6 and its discussion below). In the case of the sample $PE_{41}M_{26}A_{33}$ where the PE amounts to just 41% of the sample, the Avrami index reduces to values of just 1 or lower as shown in Figure 5a. There is a clear trend shown in Figure 5b of the Avrami index to strongly reduce as the CNT content increases when data is taken at a constant isothermal crystallization temperature of 127 °C. Values of the Avrami index lower than 1.5 are unusual and difficult to explain (for polymeric samples) in terms of a reduction in dimensionality since at least two dimensions are present when polymers crystallize in lamellar aggregates (in fact the presence of lamellae was demonstrated by TEM in ref 25). Therefore, a minimum Avrami index of 2 should be the expectation based on the morphology observed. Values of Avrami index of 1 in the classical interpretation of the Avrami equation would correspond to one-dimensional crystal structure (such as needles) growing from instantaneous nuclei. In any case, mathematical Avrami fits to the data are sometimes obtained while a physical interpretation of the data is not always possible.

As the CNT content increases, since they are very small in diameter and with a high aspect ratio, their percolation will probably occur at values below or around 5%. Therefore, a

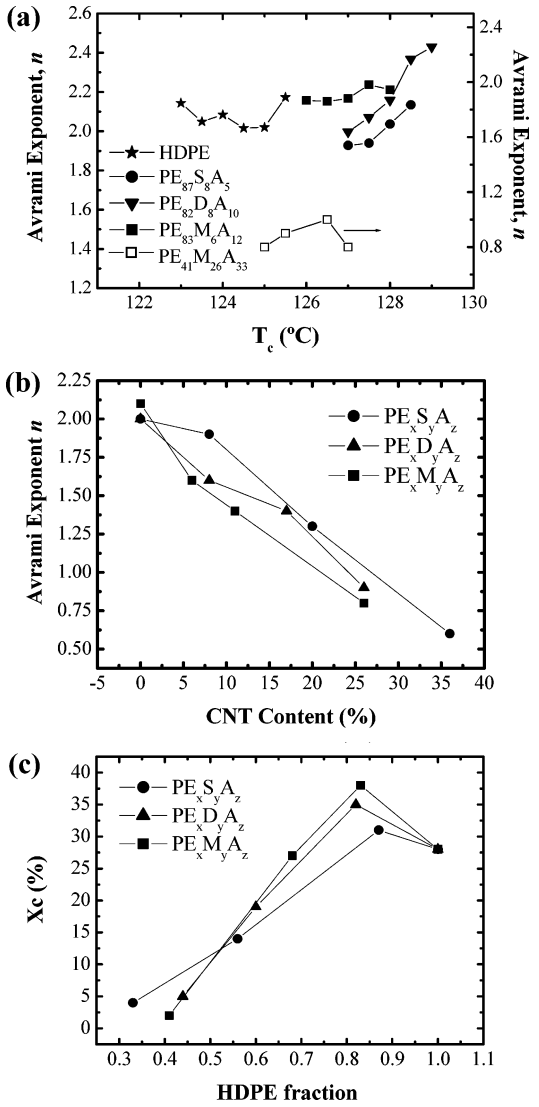

Figure 5. (a) Avrami exponent, n, as a function of isothermal crystallization temperature for selected HDPE/CNT nanocomposites. (b) Avrami exponent, n, as a function of CNT content in the nanocoposites at constant crystallization temperatute of 127 °C. (c) Degree of crystallinity obtained after isothermal crystallization at 127 °C as a function of HDPE fraction.

network of highly percolated CNT is created at higher CNT contents, that has a strong interaction with the HDPE matrix through the peculiar morphology induced by the in situ polymerization. Previous self-nucleation studies demonstrated that CNT can be up to 400% more efficient that even HDPE self-nuclei.[25] Under those circumstances, one may speculate that a situation where nucleation is the rate-determining step may arise, leading to a first-order kinetics or the equivalent of having an Avrami index close to 1. A change from nucleation and growth kinetics to a purely nucleation kinetics control might be then envisaged when the content of CNT is higher than approximately 10%. Another related situation where first-order kinetics also occurs is in diblock copolymers where isolated phases, like spheres are produced.[43] In both cases, a confinement of polymer chains can be considered to exist, in the nanocomposite case in view of the topological restrictions caused by chain interactions with the nanofiller and in the block copolymer case because of the isolated nature of the nanophases produced.[43,44]

The decrease of the Avrami index with CNT content shown in Figure 5b occurs more or less in the same way (i.e., the slope

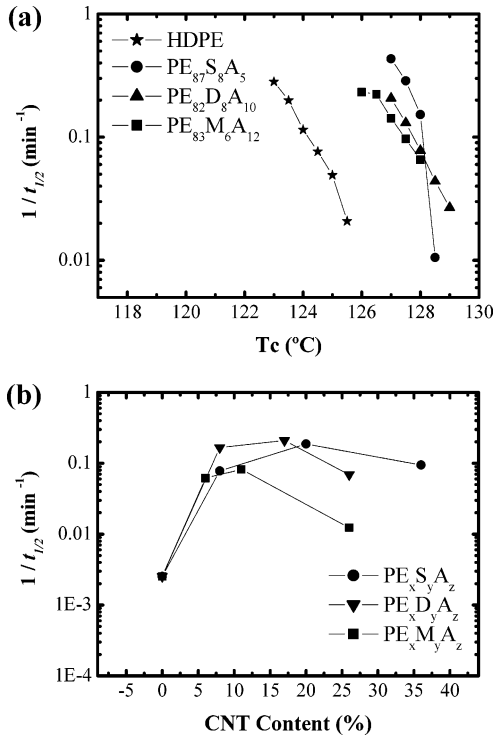

Figure 6. (a) Experimentally determined overall crystallization rate expressed as the inverse of half crystallization time as a function of the isothermal crystallization temperature for selected nanocomposite systems. (b) Inverse of half crystallization time as a function of CNT content at constant crystallization temperature for each system evaluated (see text).

in the three plots shown is very similar) regardless of the type of CNT employed (SWNT, DWNT, or MWNT).

A very interesting complementary result shown in Figure 5c is the variation of the final or saturation crystallinity achieved during isothermal crystallization at 127 °C for all samples. An initial increase in the crystallinity degree is observed at low CNT contents which can be attributed to the nucleation effect that CNT have on the HDPE matrix. However, as the CNT content increases a strong depression in crystallinity is obtained and nanocomposites with 25% CNT or more end up with crystallinity values of 5% or lower. These results are also consistent with previous results obtained under nonisothermal conditions and reported in Table 1, where the total crystallinity degree decreases as the CNT (and alumina) content increases (although not as dramatically as in the isothermal case), presumably by the increased molecular interference with crystal growth caused by high aspect ratio of CNT and their interaction with PE molecules, as discussed above. It has been previously reported in the literature that when the matrix and the nanofillers have strong interactions, such interactions can lead to decreases in crystallinity by topological confinement of macromolecular chains at the interfaces (see refs 24, 44, and 45). Torkelson et al.[46−49] have elegantly demonstrated in amorphous thin films and in model nanocomposites that when polymer−surface strong interactions exist at a molecular scale the T_g of the polymer can rise up to 40−50 °C as a consequence of chain confinement. Also, physical aging effects can decrease almost to the point of disappearance because of such chain confinement effects.[50,51] In another recent work, the inclusion of fullerenes in PMMA has also lead to increases in T_g.[52]

Since the Avrami treatment determines the crystallization kinetics relative to terms to the crystallinity saturation levels (since relative crystalline fractions are always employed[41,42]), the results of Figure 5c are worth taken into account when analyzing the values of the relative crystallization rates obtained.

Figure 6 shows the inverse of the experimental half-crystallization time, a quantity that represents the overall crystallization rate (including both nucleation and growth) as a function of isothermal crystallization temperature for nanocomposites with low amounts of CNT. In all cases, the crystallization rate is seen to decrease as T_c increases as expected since the crystallizations kinetics is dominated by primary and secondary nucleation in temperature regions close to T_m, where diffusion is not so important.[42]

The HDPE sample needs a much larger supercooling than the nanocomposite materials in order to crystallize. The acceleration of the crystallization kinetics exhibited by the nanocomposites samples is due to the nucleation effect of CNT on the HDPE matrix. When the nanocomposite materials with low CNT contents are compared, even though the crystallization rates are not so different, the following order in overall crystallization rate can be observed: PE/SWNT > PE/DWNT > PE/MWNT. Such an order reflects the surface area interaction between the different types of CNT and HDPE and therefore their nucleating action, as expected the CNT with the larger exposed area per unit volume is the SWNT, followed by the DWNT and MWNT.

The dependence of the overall crystallization rate (expressed as the inverse of the half crystallization time) on the CNT content at a specific isothermal crystallization temperature of 127 °C is shown in Figure 6b. In all cases, regardless of the CNT type, the overall crystallization rate increases with CNT content until it saturates at 15% or larger CNT contents. The reason for the increase in overall crystallization rate as compared to HDPE is the nucleation effect of the CNT that evidently saturates at high CNT contents. It must be remembered that even though the overall crystallization rate is the same, at high CNT contents the final crystallinity achieved by the sample is much smaller (see Figure 5c).

Another measure of the overall crystallization rate is the value of K or the overall crystallization rate constant provided by the fitting of the Avrami equation to the isothermal crystallization data. Parts a and b of Figure 7 show that analogous results to those obtained by representing the experimental value of the inverse of half-crystallization times are obtained. Furthermore, since K has units of min^{-n}, one must be cautious when comparing K values with different Avrami indexes (see Figure 5b), therefore we have represented in Figure 7c the values of K^{-n}, a quantity expressed in the same units regardless of the Avrami index (e.g., min^{-1}). As Figure 7c shows, the trends are the same as those in Figure 7b.

Haggenmueller et al.[14] prepared HDPE/SWNT nanocomposites by a hot coagulation method. They also found a nucleating effect of SWNT on HDPE and reductions in the Avrami index values from 2.5 to 3 to approximately 1.6 with the inclusion of 1% CNT. On the contrary, Grady et al.[16] reported increases in the Avrami index from 2.2 for neat isotactic polypropylene (PP) to 2.8 for PP/SWNT nanocomposites, however, the changes could not be ascribed to a particular supercrystalline geometry.

3.3. Wide-Angle X-ray Scattering (WAXS). The evolution of crystallization with time under isothermal conditions that mimic DSC experiments was determined by WAXS thanks to the high-energy X-ray beam of a synchrotron radiation source. The samples were first measured at room temperature, then they were heated to 170 °C in order to erase all crystalline memory (the samples remained in the melt for 3 min) and then they

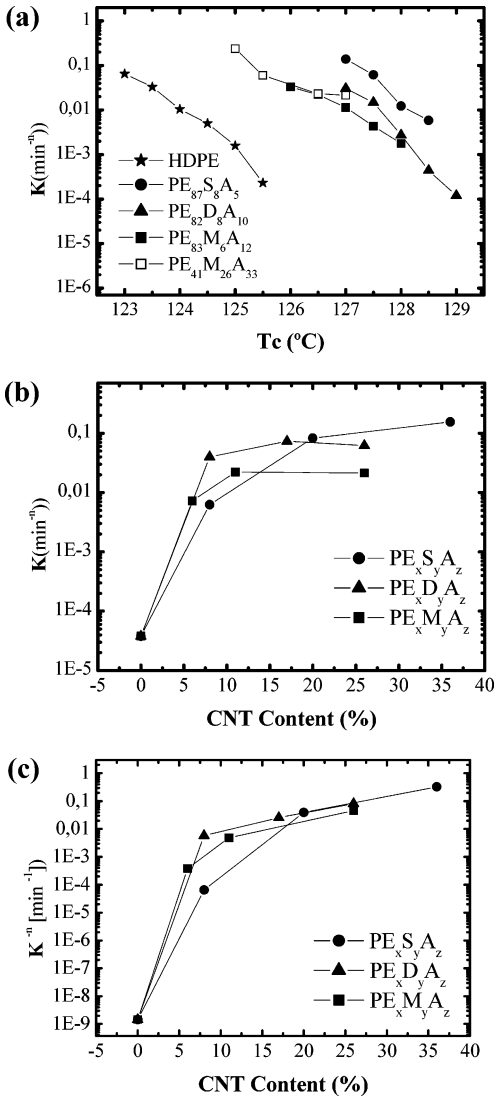

Figure 7. (a) Avrami overall crystallization rate constant, K, as a function of the isothermal crystallization temperature for selected nanocomposite systems. (b) K as a function of CNT content at constant crystallization temperature for each system evaluated (see text). (c) Avrami overall crystallization rate constant raised to the n power, K^n, at constant crystallization temperature for each system evaluated (see text).

were quickly quenched to the isothermal crystallization temperature (123.5 °C for HDPE, 126.5 °C for $PE_{83}M_6A_{12}$ and 127.5 °C for $PE_{87}S_8A_5$) where they remain until the crystallinity saturated. WAXS diffractograms were taken every 15 s.

The results obtained by WAXS indicate that the crystal structure of HDPE remains unchanged (orthorhombic unit cell) in the nanocomposites in spite of the peculiar morphology CNT can induce (i.e., bottle-brush morphology). We obtained similar results employing standard WAXS measurements.[25]

Figure 8a presents one example of the real time behavior observed with $PE_{83}M_6A_{12}$. The sample exhibits at room temperature two main reflections that are characteristic of HDPE. The highest intensity peak at 21.03° and the second most intense peak at 23.49° correspond to the (110) and (200) reflections from the orthorhombic unit cell of PE. Both reflections disappear upon melting and are replaced by the scattering of the melt phase. Later, at the isothermal crystallization temperature (126.5 °C), both reflections appear and gradually increase their intensity as time elapses.

From data analogous to that shown in Figure 8a, the isothermal crystallization kinetics can be followed by using the

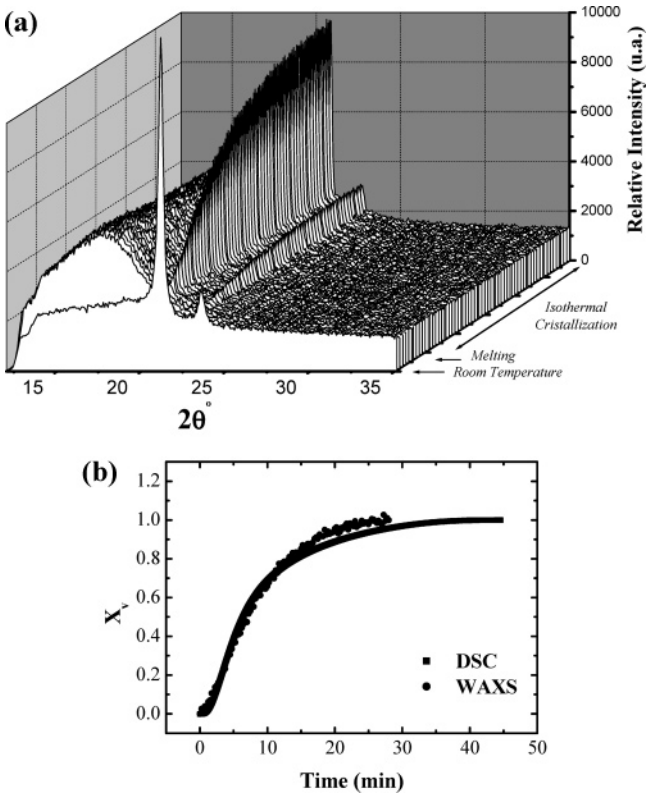

Figure 8. (a) Synchrotron real time WAXS data for $PE_{83}M_6A_{12}$. (b) Transformed volumetric fraction for HDPE obtained by DSC and WAXS after isothermal crystallization at 123.5 °C.

intensity variation as a function of time of the (100) reflection. Figure 8b shows a plot of relative crystallinity obtained by both WAXS and DSC at the same isothermal crystallization temperature for neat HDPE. A good match was obtained although the number of experimental data points was always smaller for WAXS. Therefore, we prefer to employ the DSC data for the determination of the Avrami crystallization kinetics fitting as presented above. Nevertheless, the WAXS experiments with high-energy radiation source were useful in general to corroborate the DSC findings and the lack of structural changes in the HDPE when it is forming part of the nanocomposite materials prepared by in situ polymerization.

4. Conclusions

The SSA thermal fractionation procedure applied to HDPE/CNT nanocomposites revealed that marked differences exist between the HDPE that constitutes the matrix of the nanocomposites and neat HDPE polymerized under the same conditions. The strong matrix−filler interactions induce a bottle-brush morphology where lamellae are nucleated by the CNT. As a result, a new fraction that melts at higher temperatures is produced in the nanocomposites that is not present in neat HDPE or in physically blended HDPE and MWNT. Also, a higher melting temperature (and also a higher amount as indicated by the increase in area of thermal fraction 1) is induced in the most important thermal fraction of HDPE that corresponds to more thermodynamically stable crystals induced by the nucleating action of the CNT.

The isothermal crystallization studies indicate that crystallization kinetics is accelerated by the nucleating action of CNT. For nanocomposite materials with low CNT contents the following order in overall crystallization rate was observed: PE/SWNT > PE/DWNT > PE/MWNT, even though the differences were not very large in between them. This order reflects

the filler−matrix interaction between the different types of CNT and HDPE and therefore their nucleating action, as expected the CNT with the larger exposed area per unit volume is the SWNT, followed by the DWNT and MWNT.

The interaction between the HDPE chains and the surface of the CNT is probably very strong even though it is only physical in nature. When the total crystallinity achieved during isothermal crystallization is considered as a function of CNT content, it was found that a competition between nucleation and topological confinement could account for the results. At low CNT content, the crystallinity increases, however, at higher CNT content there is a dramatic reduction in crystallinity reflecting the increased confinement experienced by the HDPE chains at the interfaces which are extremely large in these nanocomposites. Another consequence of these strong interactions is the remarkable decrease in Avrami index as CNT content increases. When the Avrami index reduces to 1 or lower, nucleation dominates the overall kinetics as a consequence of confinement effects. Wide-angle X-ray experiments confirmed the isothermal crystallization results obtained by DSC and also demonstrated that no change in the orthorhombic unit cell of HDPE occurred during crystallization with or without CNT.

Acknowledgment. The USB team acknowledges finantial support from the Decanato de Investigación y Desarrollo of Simón Bolívar University through Grant GID-G02. CIRMAP thanks Nanocyl S.A. (Sambreville, Belgium) for kindly providing the carbon nanotubes. This work was financially supported by "Région Wallonne" and European Community (FEDER, FSE) within the framework of ''Objectif 1: Materia Nova''. CIRMAP thanks the "Belgian Federal Government Office Policy of Science (SSTC)" for general support in the frame of the PAI-5/03. S.B. thanks the "European Community" for financial support in the framework of the Nanohybrid project (STREP NMP3-CT-2005-516972).

References and Notes

(1) Ajayan, P. M. *Handbook of Nano-structured Materials and Nanotechnology*; Nalwa, H. S., Ed.; Academic Press: San Diego, CA, 2000, Vol. 5; Chapter 6, p 575.
(2) Wang, C.; Guo, Z-X.; Fu, S.; Wu, W; Zhu, D. *Prog. Polym. Sci.*. **2004**, *29*, 1079.
(3) Ajayan, P. M.; Zhou, O. Z. *Top. Appl. Phys.* **2001**, *80*, 391.
(4) Moniruzzaman, M.; Winey, K. I. *Macromolecules* **2006**, *39*, 5194.
(5) Bonduel, D.; Alexandre, M.; Monteverde, F.; Dubois, P.; Mainil, M. *Chem. Commun.* **2005**, *6*, 781.
(6) Enikolopian, N. S. USSR Pat. 763,379, 1976.
(7) Howard, E. G.; US Pat, 4,097,447, 1978.
(8) Kaminsky, W.; Zielonka, H. *Polym. Adv. Technol.* **1993**, *4*, 415.
(9) Alexandre, M.; Martin, E.; Dubois, P.; Garcia-Marti, M.; Jérome, R. *Macromol. Rapid Commun.* **2000**, *21*, 931.
(10) Alexandre, M.; Martin, E.; Dubois, P.; Garcia-Marti, M.; Jérome, R. *Macromol. Chem. Mater.* **2001**, *13*, 236.
(11) Alexandre, M.; Pluta, M.; Dubois, P.; Jérome, R. *Macromol. Chem. Phys.* **2001**, *202*, 2239.
(12) Mahfuz, H.; Adnan, A.; Rangari, V. K.; Jeelani, S. *Int. J. Nanosci.* **2005**, *4*, 55.
(13) Chen, Q.; Bin, Y.; Matsuo, M. *Macromolecules* **2006**, *39*, 6528.
(14) Haggenmueller, R.; Fisher, J. E.; Winey, K. I. *Macromolecules* **2006**, *39*, 2964.
(15) Bhattacharyya, A. R.; Sreekumar, T. V.; Liu, T.; Kumar, S.; Ericson, L. M.; Hauge, R. H.; Smalley, R. E. *Polymer* **2003**, *44*, 2373.
(16) Grady, B. P.; Pompeo, F.; Shambaugh, R. L.; Resasco, D. E. *J. Phys. Chem. B* **2002**, *106*, 5852.
(17) Assouline, E.; Lustiger, A.; Barber, A. H.; Cooper, C. A.; Klein, E.; Wachtel, E.; Wagner, H. D. *J. Polym. Sci., Part B: Polym. Phys.* **2003**, *41*, 520.
(18) Probst, O.; Moore, E. M.; Resasco, D. E.; Grady, B. P. *Polymer* **2004**, *45*, 4437.
(19) Minus, M. L.; Chae, H. G.; Kumar, S. *Polymer* **2006**, *47*, 3705.
(20) Michell, C. A.; Krishnamoorti, R. *Polymer* **2005**, *46*, 8796.
(21) Ryan, K. P.; Lipson, S. M.; Drury, A.; Cadek, M.; Ruether, M.; O'Flaherty, S. M.; Barron, V.; McCarthy, B.; Byrne, H. J.; Blau, W. J.; Coleman, J. N. *Chem. Phys. Lett.* **2004**, *391*, 329.
(22) Bin, Y.; Kitanaka, M.; Zhu, D.; Matsuo, M. *Macromolecules* **2003**, *36*, 6213.
(23) Goh, H. W; Goh, S. W.; Xu, G. Q.; Pramoda, K. P.; Zhang, W. D. *Chem. Phys. Lett.* **2003**, *379*, 236.
(24) Chatterjee, T.; Yurekli, K.; Hadjiev, V. G.; Krishnamoorti, R. *Adv. Funct. Mater.* **2005**, *15*, 1832.
(25) Trujillo, M.; Arnal, M. L.; Müller, A. J.; Laredo, E.; Bredeau, St.; Bonduel, D.; Dubois, Ph. *Macromolecules* **2007**, *40*, 6268.
(26) Bao, S. P.; Tjong, S. C. *Mater. Sci. Eng.* **2007**, in press. doi:10.1016/j.msea.2007.08.050.
(27) Anand, K. A.; Agarwal, U. S.; Joseph, R. *Polymer* **2006**, *47*, 3976.
(28) Gao, Y.; Wang, Y.; Shi, J.; Bai, H.; Song, B. *Polym. Test.* **2007**, in press. doi;10.1016/j.polymertesting. 2007.09.012.
(29) Chen, E-C.; Wu, T-M. *Polym. Degrad. Stab.* **2007**, *92*, 1009.
(30) Jin, J.; Song, M.; Pan, F. *Thermochim. Acta* **2007**, *456*, 25.
(31) Bonduel, D.; Bredeau, S.; Alexandre, M.; Monteverde, F.; Dubois, Ph. *J. Mater. Chem.* **2007**, *17*, 2359.
(32) Lorenzo, A. T.; Arnal, M. L.; Sánchez, J. J.; Müller, A. J. *J. Polym. Sci., Part B: Polym. Phys.* **2006**, *44*, 1738.
(33) Fillon, B.; Wittmann, J. C.; Lotz, B.; Thierry, A. *J. Polym. Sci., Part B : Polym. Phys.* **1993**, *31*, 1383.
(34) Müller, A. J.; Arnal, M. L. *Prog. Polym. Sci.* **2005**, *30*, 559.
(35) Müller, A. J.; Hernández, Z. H.; Arnal, M. L.; Sánchez, J. J. *Polym. Bull. (Berlin)* **1997**, *39*, 465.
(36) Arnal, M. L.; Balsamo, V.; Ronca, G.; Sánchez, A.; Müller, A. J.; Cañizales, E.; Urbina de Navarro, C. *J. Therm. Anal. Calor.* **2000**, *59*, 451.
(37) Lorenzo, A. T.; Arnal, M. L.; Müller, A. J.; Boschetti de Fierro, A.; Abetz, V. *Macromol. Chem. Phys.* **2006**, *207*, 39.
(38) Arnal, M. L.; Cañizales, E.; Müller, A. J. *Polym. Eng. Sci.* **2002**, *42*, 2048.
(39) Arnal, M. L.; Sánchez, J. J.; Müller, A. J. *Polymer* **2001**, *42*, 6877.
(40) Balsamo, V.; Urdaneta, N.; Pérez, L.; Carrizales, P.; Abetz, V.; Müller, A. J. *Eur. Polym. J.* **2004**, *40*, 1033.
(41) Shultz, J. *Polymer Materials Science*; Prentice Hall, Inc.: New Jersey, **1974.**
(42) Lorenzo, A. T.; Arnal, M. L.; Albuerne, J.; Müller, A. J. *Polym. Test.* **2007**, *26*, 222.
(43) Müller, A. J.; Balsamo, B.; Arnal, M. L. *Adv. Polym. Sci.* **2005**, *190*, 1. 77. Müller, A. J.; Balsamo, V.; Arnal, M. L.; Jakob, T.; Schmalz, H.; Abetz, V. *Macromolecules* **2002**, *35*, 3048. 137. Lorenzo, A. T.; Arnal, M. L.; Müller, A. J.; Boschetti-de-Fierro, A.; Abetz, V. *Macromolecules* **2007**, *40*, 5023.
(44) Kuppa, V.; Menakanit, S.; Krishnamoorti, R.; Manias, E. *J. Polym. Sci., Part B: Polym. Phys.* **2003**, *41*, 3285.
(45) Lincoln, D. M.; Vaia, R. A.; Krishnamoorti, R. *Macromolecules* **2004**, *37*, 4554.
(46) Priestley, R. D.; Broadbelt, L. J.; Torkelson, J. M.; Fukao, K. *Phys. Rev. E* **2007**, *75*, 061806.
(47) Rittigstein, P.; Priestley, R. D.; Broadbelt, L. J.; Torkelson, J. M. *Nature Mat.* **2007**, *6*, 278.
(48) Roth, C. B.; McNerny, K. L.; Jager, W. F.; Torkelson, J. M. *Macromolecules* **2007**, *40*, 2568.
(49) Mundra, M. K.; Donthu, S. K.; Dravid, V. P.; Torkelson, J. M. *Nano Lett.* **2007**, *7*, 713.
(50) Priestley, R. D.; Rittigstein, P.; Broadbelt, L. J.; Fukao, K.; Torkelson, J. M. *J. Phys.: Condens. Matter.* **2007**, *19*, 205120.
(51) Mundra, M. K.; Ellison, C. J.; Rittigstein, P.; Torkelson, J. M. *Eur. Phys. J. Special Topics* **2007**, *141*, 143.
(52) Kropka, J. M.; Putz, K. W.; Pryamitsyn, V.; Ganesan, V.; Green, P. *Macromolecules* **2007**, *40*, 5424.

MA702272E